Numerical modelling of the gravity-induced destabilization of a slope: The example of the La Clapière landslide, southern France

A.I. Chemenda, T. Bois *, S. Bouissou, E. Tric

Geosciences Azur, Université de Nice Sophia-Antipolis and CNRS, Valbonne, France

ARTICLE INFO

ABSTRACT

A finite difference two-dimensional model with Hooke–Mohr–Coulomb properties and topography derived from the DEM are used to reproduce the La Clapière landslide. The principal factor defining the gravity-driven destabilization of the model is a gradual reduction in the cohesion. This reduction simulates a degradation of the material properties with time because of weathering/alteration processes. The inelastic deformation, fracturing, and faulting first occur at mountain scale and results in normal fault formation causing crest sagging. Later, the failure process is concentrated in the lower part of the slope and leads to the formation of a localized fault subparallel to the slope surface at a depth of ca. 100 m. This corresponds to the initiation of the La Clapière landslide and its propagation upslope. A slow crest sagging continues during the whole model evolution.

© 2009 Elsevier B.V. All rights reserved.

1. Introduction

Gravitational instability of topography results from the interplay of different processes. The most important seems to be the weathering and alteration caused by climatic factors and fluid circulation within the massif and dependent on the physicochemical and mechanical properties of the rock (Hill and Rosenbaum, 1998; Hall and André, 2001; Pellegrino and Prestininzi, 2007). Both weathering and alteration cause a progressive time-softening (strength reduction) of the superficial horizons. Although the kinematics of these processes and their variation with depth are poorly studied, the softening is generally maximal at the surface and diminishes with depth (Chigira, 2001; Maréchal et al., 2003) where it is concentrated along the fractures and faults (Migon and Lidmar-Bergstroem, 2002; Wyns, 2002).

Ignoring the influence of other factors (e.g., large spatial and temporal scale tectonic processes) on the slope evolution, we assume the following conceptual model: the initially homogeneous and stable mountain is subject to a progressive reduction of effective strength because of rock weathering and alteration. Ultimately, this mountain should undergo inelastic, gravity-driven deformation (damage) and macrofracturing increasing with time. The aim of the present work is to model this deformation numerically and compare the results with field data. Lack of similarity would mean that the conceptual model is too simplistic and that in reality other factors (e.g., structural heterogeneities, tectonic stresses, and more complex mechanical properties) have a dominant role in controlling the gravity-induced deformation.

The well-studied La Clapière landslide (Follacci, 1987, 1999; Ivaldi et al., 1991; Guglielmi et al., 2002; Casson et al., 2005; Lebourg et al., 2005; Jomard, 2006) located in the southern French Alps (Argentera–Mercantour massif) was chosen as a natural example (Fig. 1). The numerical models well reproduce this superficial landslide (its depth, size, and along-slope position) and also reveal slower inelastic deformation (normal faulting) at a larger scale involving the whole mountain and resulting in crest sagging.

2. Geological framework

The La Clapière slope (Figs. 1 and 2A) is situated in the Tinée valley, which represents the north-western edge of the Argentera–Mercantour metamorphic unit (southern French Alps). The region underwent polyphased tectonic deformations during Variscan and Alpine orogenesis (Follacci, 1999). The eastern side of the valley is mainly made of weathered metamorphic units characterized by a N. 150–60° E. foliation (average trend) (Bogdanoff, 1986; Gunzburger and Laumonier, 2002) with the dip varying with depth (Follacci, 1987; Gunzburger and Laumonier, 2002; Delteil et al., 2003) in the landslide area (Fig. 2C).

The La Clapière landslide overlaps the Quaternary alluvial deposits of the Tinée River and can be considered as a highly permeable fractured reservoir drained at the bottom by a group of perennial springs (Fig. 1). The whole La Clapière slope can be divided into

---

* Corresponding author. Tel.: +33 492 942 620; fax: +33 492 942 610.
E-mail address: bois@geoazur.unice.fr (T. Bois).
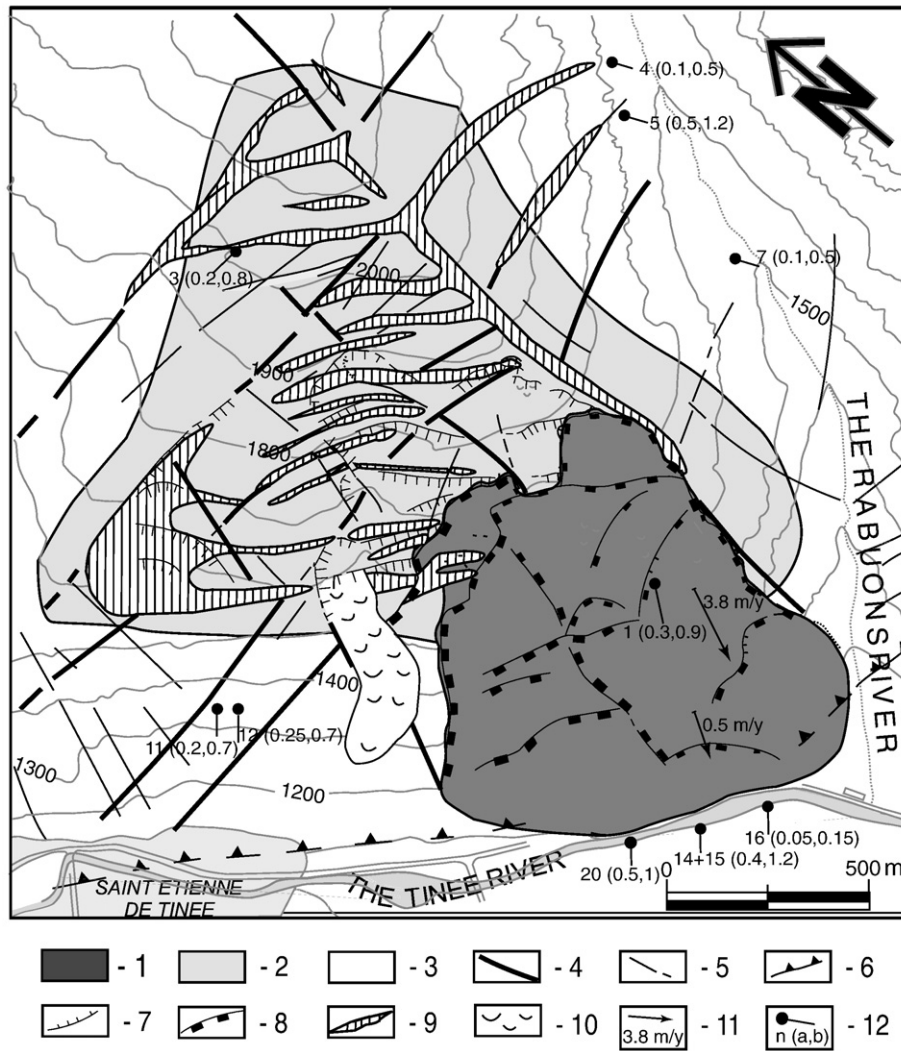
Fig. 1. Structural and hydrological framework of the La Clapière landslide (simplified after Guglielmi et al., 2005). 1, La Clapière landslide; 2, uncompressed toppled zone ($10^{-3} > K > 10^{-5}$ m/s); 3, low uncompressed zone ($10^{-8} > K > 10^{-9}$ m/s); 4, major normal faults; 5, minor faults; 6, thrust fault; 7, old scarps; 8, present day scarp; 9, crevices deposit ($10^{-2} > K > 10^{-3}$ m/s); 10, debris flow; 11, velocity vector with 1996 annual velocity value; 12, perennial spring with water table flow rate, n is the number of the spring, a is the minimal, and b is the maximal flow rate values in l/s.

a low uncompressed zone at depth and a decompression highly fractured toppled zone where tensile crevices create linear drains with estimated hydraulic conductivity K ranging between 10^{-2} and 10^{-3} m/s (Fig. 1).

The slope is fractured by three nearly vertical sets of tectonic faults, trending N. 010° E.–N. 030° E., N. 080° E.–N. 090° E., and N. 110°E.–N. 140° E. (Fig. 1). The details of faulting in the present landslide area are shown in Fig. 2B. The material in this zone is intensively weathered to depths of at least 200 m (Guglielmi et al., 2005) and hence underwent mechanical degradation, although no quantitative information about this is available.

Fig. 3 shows that in 1938 the La Clapière landslide was at its very initial stage. The recent activation of the deformation, which probably shaped the current sliding unit, started in 1950–1955 with the sliding velocity progressively increasing to the maximal value of 6 m/year in 1987. After that the velocity decreased and varied with time from 4 to 2 m/year (Guglielmi et al., 2005). It is not homogeneous along the slope either (Casson et al., 2005; see also Fig. 1). According to the geological data (Merrien-Soukatchoff and Gunzburger, 2006) the landslide propagates upslope, which can also be seen in Fig. 3.

3. Numerical modelling

Accurate numerical simulation of gravitational instability (as of any other physical instability) is a delicate exercise. It requires application of a "time-marching" explicit solution scheme. Such a scheme is implemented in the dynamic, finite-difference calculation code FLAC3D. This code also uses mixed-discretization zoning technique that is believed to ensure accurate modelling of plastic collapse loads and plastic flow (Marti and Cundall, 1982). Therefore FLAC3D has been chosen for the numerical simulations presented below.

3.1. Setup of numerical simulations and the constitutive model

We simulate the gravity-driven, plane-strain deformation of a two-dimensional model with roller boundary conditions along the model bottom and the vertical borders (Fig. 4A). Such boundary conditions are typically used in the numerical models of landsliding (e.g., Helmstetter et al., 2004; Ambrosi and Crosta, 2006; Hermanns et al., 2006). These conditions imply that at the timescale of the process under consideration (landsliding), the tectonic horizontal displacement is negligible. The tectonic stresses are ignored as well. The
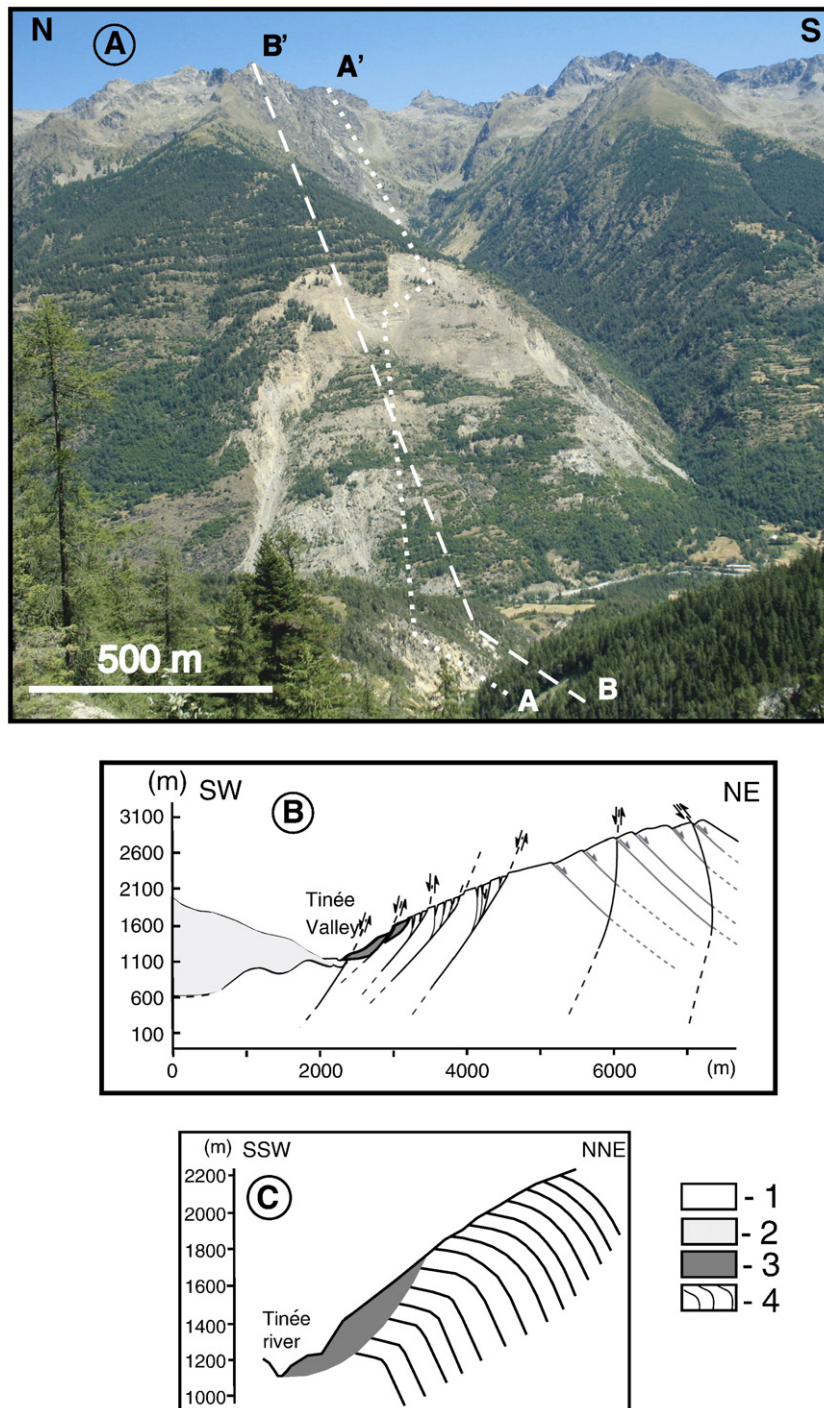
Fig. 2. The Clapière landslide. (A) Photo of the landslide taken in 2008 (courtesy of G. Sanchez); (B) simplified geological section (from (Jomard, 2006)) along the profile AA′ in Fig. 2A; (C) toppling of the foliation in the landslide area (simplified and modified after (Gunzburger et Laumonier, 2002)). 1, metamorphic basement; 2, sedimentary deposits; 3, the La Clapière landslide; 4, the foliation. BB′ corresponds to the topographic profile used in the numerical models.

vertical boundaries themselves are set at the valley and the crest axes, which are thus considered as the axes of symmetry: the underlying assumption is, strictly saying, that the topography is periodic and that the model corresponds to its half-wavelength. The roller condition at the model bottom means that the model bottom is free to move in the horizontal direction that simulates the effect of the infinitely thick object: the model bottom, which is an artificial (not natural) boundary, is not attached to the infinitely rigid basis (is not fixed) but to the infinitely thick substratum with the same elastic rigidity

as the model. Because it is infinitively thick, its resistance to the horizontal displacement of the model is small.

The model topography (free surface) is extracted from an SRTM file (referred to as SRTM_38_04), along the profile BB′ defined in Fig. 2A. The model has homogeneous elastic-plastic properties described by Hooke's equations:

$$d\varepsilon_{ij}^{e} = \frac{d\sigma}{K}\delta_{ij} + \frac{ds_{ij}}{2G} \qquad (1)$$
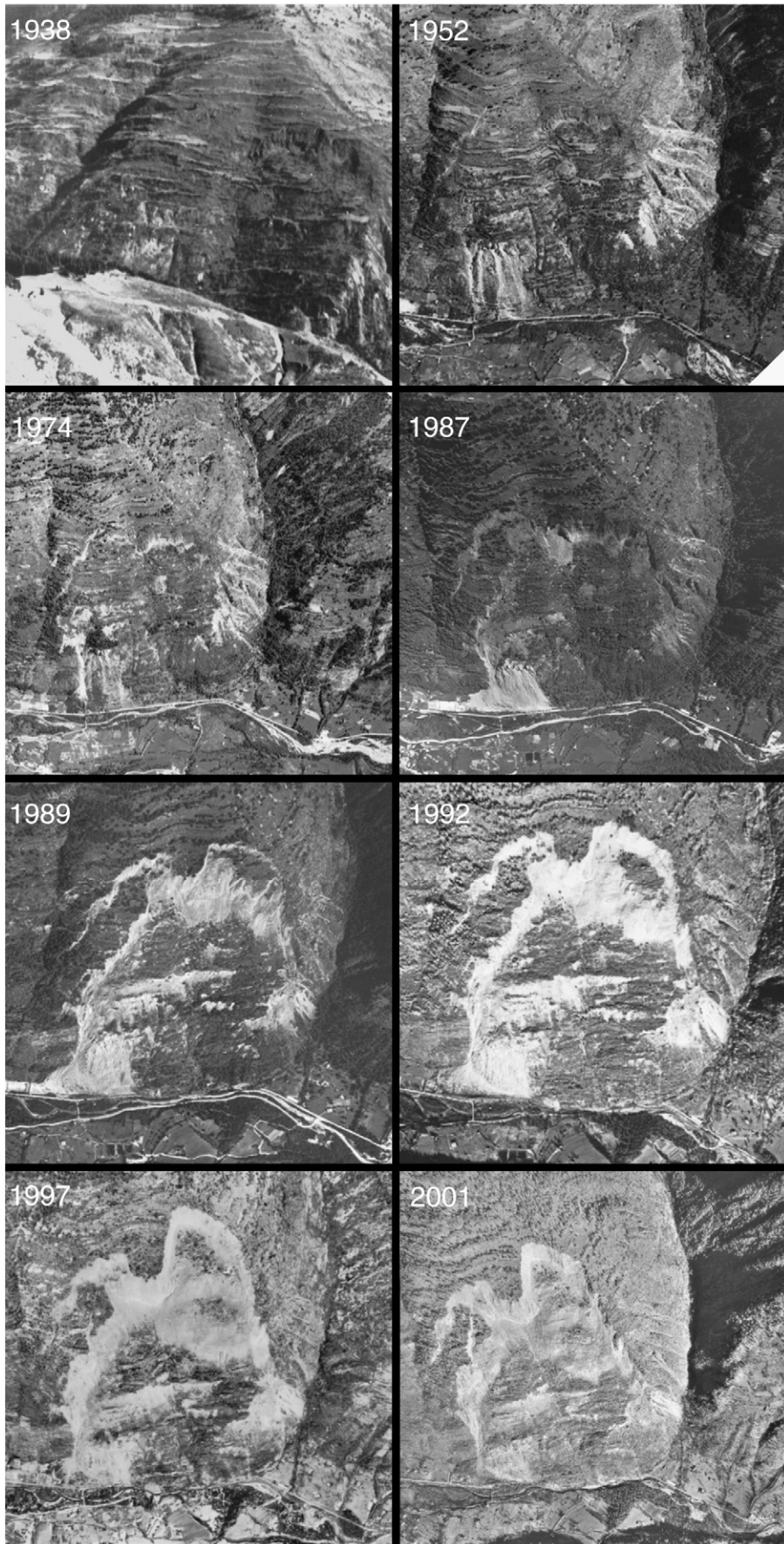
Fig. 3. Snapshots of the La Clapière zone showing the landslide evolution from 1938 to 2001. The 1938 picture is taken from a postcard provided by Y. Gunzburger. The 1952–2001 photos are from the Web site: http://www.lithotheque.ac-aixmarseille.fr/Affleurements_PACA/clapiere_06/CLAP_HISTOIRE.htm.
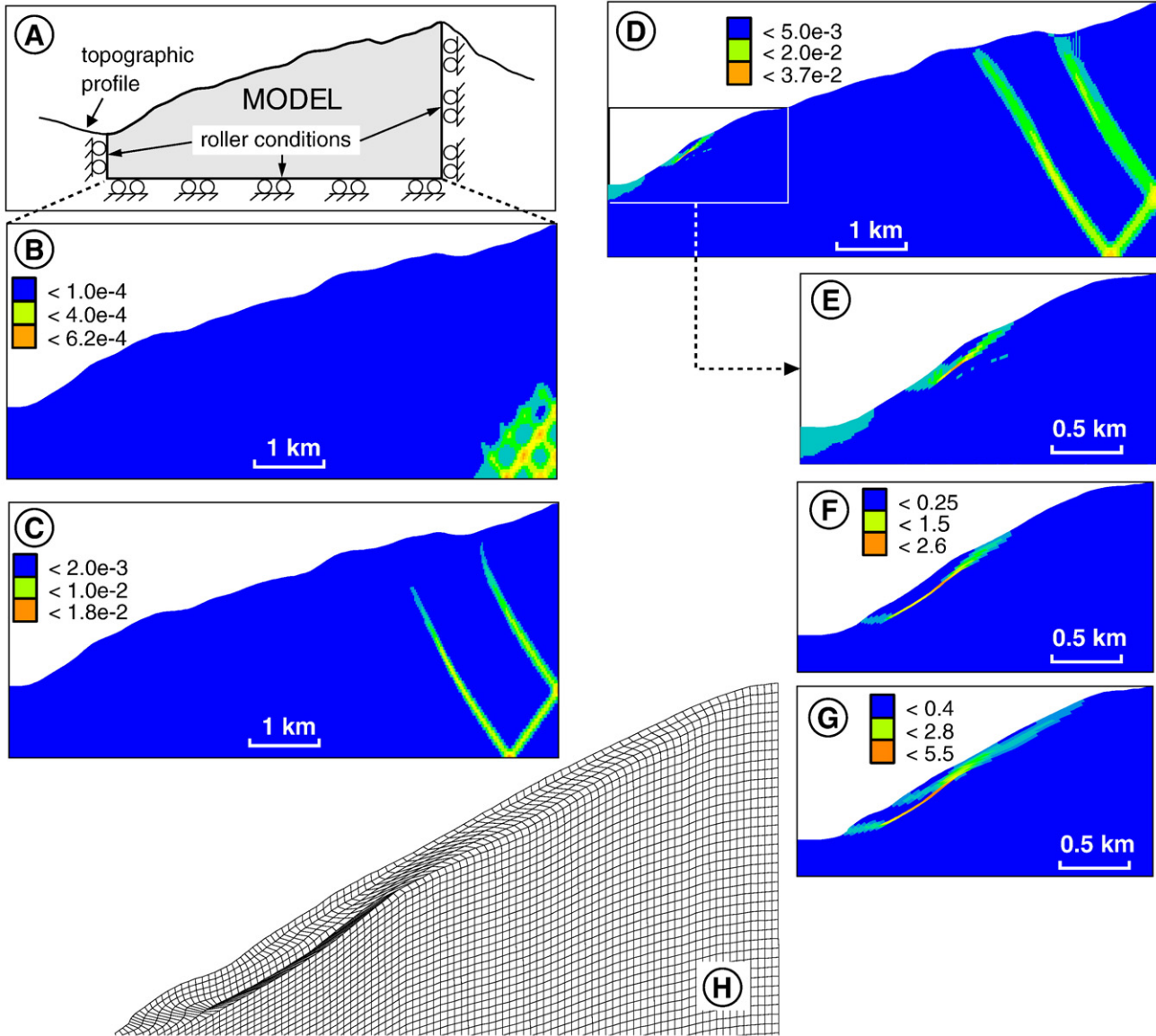
Fig. 4. Evolution of the numerical model for $\phi=30°$ during progressive reduction of the cohesion. (A) setup; (B) to (G) stages of the model evolution; (H) deformed grid corresponding to the stage (G) and showing the bending (toppling) of the initially vertical grid lines. Grey-level palettes correspond to the accumulated inelastic deformation $\overline{\gamma}^{p}$ representative of the material damage degree.

and the Mohr–Coulomb yield $f(\sigma_{ij})$ and plastic potential $\Phi(\sigma_{ij})$ functions:

$$f = \sigma_1 - \sigma_3 N_\phi - 2c\sqrt{N_\phi} \qquad (2)$$

$$\Phi = \sigma_1 - \sigma_3 N_\psi - 2c\sqrt{N_\psi} \qquad (3)$$

where $N_\phi = \frac{1+\sin\phi}{1-\sin\phi}, N_\Psi = \frac{1+\sin\psi}{1-\sin\psi}, s_{ij} = \sigma_{ij} - \delta_{ij}\sigma$, is the stress deviator, δ_{ij} is the Kronecker delta, σ_{ij} is the stress, $\sigma = \frac{1}{3}\sigma_{ii}$ is the mean stress, K and G are the elastic bulk and shear modulii, σ_i are the principal stresses: $\sigma_3 \leq \sigma_2 \leq \sigma_1$; the compressive stress is positive, c is the cohesion, φ and ψ are the internal friction and dilatancy angles, correspondingly, ε_{ij}^e is the elastic strain, $i,j=1, 2, 3$, the repeated subscripts imply summation. The increments of inelastic ("plastic") strains are defined as

$$d\varepsilon_{ij}^p = d\lambda \frac{\partial\Phi}{\partial\sigma_{ij}} \qquad (4)$$

where $d\lambda$ is non-negative scalar function found at each calculation step by substituting the elastic trial stresses into the yield condition (E2). The total strain increment is

$$d\varepsilon_{ij} = d\varepsilon_{ij}^e + d\varepsilon_{ij}^p \qquad (5)$$

The history of inelastic deformation is tracked during the calculation using the effective inelastic shear strain $\overline{\gamma}^p = \int(2de_{ij}^p de_{ij}^p)^{1/2}$ where $de_{ij}^p = d\varepsilon_{ij}^p - \frac{1}{3}\delta_{ij}d\varepsilon_{kk}^p$ ($k=1, 2, 3$). This parameter characterizes (is proportional to) the material damage degree (e.g., Chen, and Han, 1988).

The grid zone size (the spatial resolution) is 20 m. Because the code uses an explicit calculation scheme, the time step is very small, but it does not have meaning of the real time in quasistatic (noninertial) calculations performed in this work. The model is initially elastically equilibrated under the gravity force with the following parameter values: the Young modulus $E=20$ GPa, the Poisson ratio $v=0.23$, and the density $\rho=2700$ kg/m³ (Merrien-Soukatchoff et al., 2001; Willenberg, 2004). After this, the internal

friction angle ϕ was set to a certain value (different in different models).

Very little data are available for the ψ values. The authors are not aware of such data for the gneisses. For the sedimentary rocks at low mean stress (corresponding to the conditions at the mountain scale), ψ varies from slightly positive to slightly negative values (Wong et al., 1997). This justifies the fact that most authors dealing with the mechanical analysis of landsliding assume ψ to be zero or do not take this parameter into account at all (e.g., Merrien-Soukatchoff et al., 2001; Ambrosi and Crosta, 2006; Hermanns et al., 2006; Merrien-Soukatchoff and Gunzburger, 2006). Such an assumption is also made in most geotechnical applications and it was adopted in this study.

The initial cohesion c_{ini} was chosen so that the initial (after equilibration) stress-state of the model is close to the yield surface, but still in the elastic domain. This value thus depends on ϕ (the greater ϕ is, the smaller the c_{ini} value will be) and is not defined by the laboratory measurements. During cycling (a model run), c is incrementally reduced throughout the whole model, while ϕ is kept constant. In different model runs, ϕ varied from 15° to 50°. We present in detail the most "successful" model, run at $\phi = 30°$ and glance through the results of the others.

3.2. Results

The preliminary numerical analysis showed that in order to maintain the model under quasi-static conditions and have stable results (with respect to the cohesion increments Δc value), Δc must be $<0.1c$ (where c is the current value of the cohesion during cycling) and should be applied each time the inelastic deformation is stopped (the new reduction in cohesion is applied when the inelastic deformation caused by the previous c reduction has ceased).

Fig. 4 presents the numerical model run at $\phi = 30°$ and $c_{ini} = 11$ MPa. At the initial stages of the model evolution, the inelastic deformation concentrates under the valley axial zone at depths of <300 m (we will call such depths shallow) and under the summit zone where the deformation rapidly localizes along two shear bands (normal faults) crossing the whole model from the base to the surface (Fig. 4B to D). This latter deformation/faulting (which we call deep) causes sagging of the mountain summit zone. The deep normal faulting starts at $c \approx 10$ MPa. When c is reduced to ~1 MPa, the failure
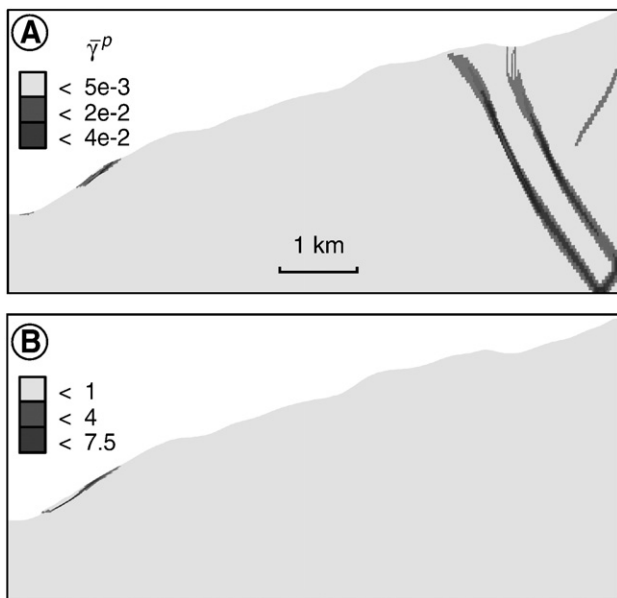
Fig. 5. Two stages of the model run at $\phi = 35°$: (A) $c = 2 \times 10^4$ Pa; (B) $c = 1 \times 10^4$ Pa. The large-scale normal faults are not seen in Fig. 5B, but they are still active. Grey-level palettes correspond to the accumulated inelastic deformation $\overline{\gamma}^p$.
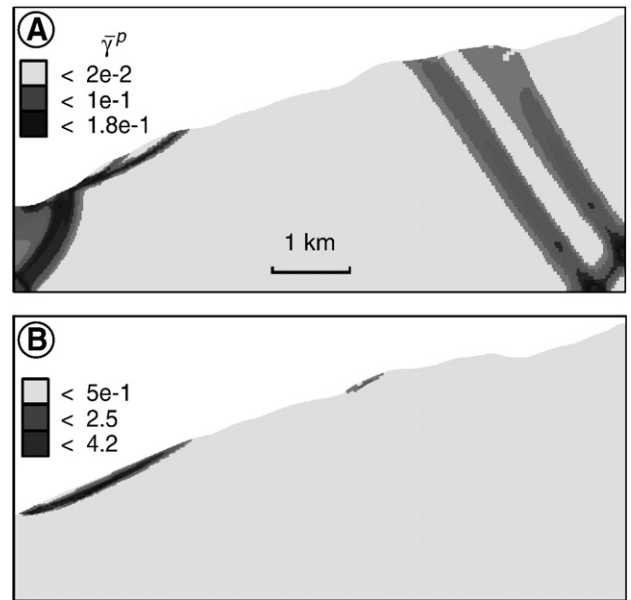
Fig. 6. Two stages of the model run at $\phi = 25°$: (A) $c = 1.6 \times 10^5$ Pa; (B) $c = 2 \times 10^4$ Pa. The large-scale normal faults are not seen in Fig. 6B, but they are still active. Grey-level palettes correspond to the accumulated inelastic deformation $\overline{\gamma}^p$.

is concentrated in the lower part of the slope and propagates from the valley axial zone up along the slope. This results in the initiation of a localized fault at a depth of ~100 m (Figs. 4D and E). The fault then propagates downslope (Fig. 4F). At this stage, the value of the cohesion is $c = 0.063$ MPa. During further reduction of c, the fracturing/failure propagates upward (Fig. 4G). At the last stage of the model evolution in Fig. 4G and H, $c \approx 0.03$ MPa. At this stage the deep normal faulting in the thickest part of the model and the associated crest sagging remain active, but the displacement along the faults is more than two orders of magnitude slower than the sliding at shallow depth.

Increase of the internal friction angle in the numerical models results in a progressive reduction of both horizontal and vertical sizes of the sliding shallow unit (Fig. 5); and at $\phi \geq 45°$, the shallow sliding does not occur at all (even at $c = 0$). But deep normal faulting resulting in crest sagging is still active (it is not displayed in Fig. 5B as the $\overline{\gamma}^p$ value along these faults is more than two orders of magnitude less than along the shallow faults). On the contrary, reduction of ϕ results in an increase of the sliding unit size (Fig. 6). The maximal depth of the sliding surface increases to ~150 m, and the deformation pattern in general becomes different: a deep thrust fault forms in the lower part of the valley (Fig. 6A) before and during the shallow sliding (one can see also a small landslide upslope in Fig. 6B). The displacement along this fault modifies the adjacent topography (before the fault formation, the altitude of the future fault zone was 1168 m but afterward it was 1228 m).
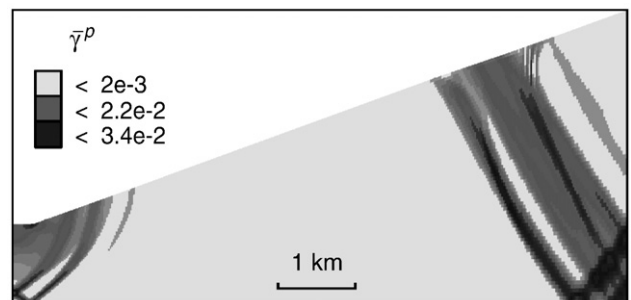
Fig. 7. Model with idealized linear topography run at $\phi = 30°$ until $c = 1 \times 10^4$ Pa. Grey-level palettes correspond to the accumulated inelastic deformation $\overline{\gamma}^p$.

Fig. 7 presents one more model with simple linear slope topography and the same mechanical parameter values as in the first model in Fig. 4. The shallow landslide does not occur in this case. This result shows that relatively small-scale topographic fluctuations/irregularities play a crucial role in triggering shallow instabilities. The reason is because these topographic features cause the stress variations of the corresponding wavelength that result in local satisfaction of the condition (E2) in certain places. Once initiated, failure will propagate according to the existent stress field. Without small-wavelength (compared to the entire slope) topographic irregularities, the variation of the stress field along the slope is gradual and failure is only possible in the areas with maximal and minimal horizontal stress that are located, correspondingly, in the valley axial and summit zones (as is the case in Fig. 5).

4. Discussion and conclusions

The simple and robust constitutive model without strain softening or hardening and with homogeneous reduction in cohesion with time has been chosen to define the first-order deformation pattern of the gravitationally destabilizing slope. As expected, this process is affected by both the slope material properties and the topography. For the topography of the La Clapière slope, the most realistic results correspond to an internal friction angle ϕ of about 30°. For this value, the maximal depth of the shallow failure/sliding surface in the model (Fig. 4) is approximately the same as in nature (Fig. 2B) of ca. 100 m. The ϕ value close to 30° was also measured in the laboratory for the rocks from the studied site (Merrien-Soukatchoff et al., 2001; Willenberg, 2004) and estimated from RMR values provided by ground mapping and Schmidt hammer tests (Gunzburger and Merrien-Soukatchoff, 2002; Gunzburger et al., 2005). A nontrivial conclusion that follows is that the scaling factor for this parameter is equal to the unity (ϕ is scale-insensitive and practically the same for a rock sample and a rock mass). The effective strength or the rock mass (hence, cohesion c) is known to be strongly scale-dependent (Arora, 1987; Hoek and Brown, 1997; Verman et al., 1997) and therefore cannot be derived directly from the laboratory measurements. It can be estimated from the modelling results.

The along-slope length l_{Cl} of the La Clapière landslide is 1400 m on average. In the model in Fig. 4, this parameter is $l_{Mod} = 1250$ m at stage (F) and $l_{Mod} = 1900$ m at stage (G). The l_{Cl} value is attained in the model between these stages, but closer to the stage in Fig. 4F that corresponds to $c = 0.063$ MPa. This value can be assumed as the minimal effective cohesion of the rocks in the La Clapière site. The maximal cohesion value at which the landslide initiates in the model is, as mentioned, ~1 MPa. Gunzburger and Merrien-Soukatchoff (2002) determined the cohesion of the rocks for the La Clapière site, using RMR methodology, to be 0.24 MPa. A direct laboratory testing of late alpine gneiss samples yields $c = 16$ MPa for intact and $c = 2$ MPa for weathered rocks (Willenberg, 2004). The c values derived from the numerical simulations are thus generally smaller than those measured on real rocks. This agrees with the well known fact that the strength (cohesion) measured in the laboratory on a small rock sample is typically considerably larger than the effective strength that characterizes a rock mass (Hoek and Brown, 1997). The low c values obtained from the numerical simulations result from the "homogenization" of the material properties in the model. In reality, they are very heterogeneous, especially because of the presence of fractures and faults where c can be reduced virtually to zero (Hajiabdolmajid et al., 2002). The fracture/fault sets can be introduced into the model (if of a tectonic origin) or generated by the gravity force as the result of a constitutive instability (Chemenda, 2007) in future more elaborate models.

As in the model in Fig. 4, the La Clapière landslide was initiated at its lower part and then extended upslope to its present limits (Follacci, 1987; Merrien-Soukatchoff and Gunzburger, 2006). The model also reproduces the toppling of the foliation associated with the landslides

in different regions (Hoek and Bray, 1991), including that of La Clapière (compare Figs. 2C and 4H). In the latter case, this feature, however, is believed to be caused by the Oligocene–Miocene folding (Gunzburger and Laumonier, 2002).

In conclusion, a good numerical reproduction of the chosen landslide using a robust model (without any complications introduced to fit the data) shows that this approach has good potential for modelling landsliding. As a first approximation, the slope destabilization does not seem to be sensitive to structural and mechanical heterogeneities (that are usually not well constrained), at least in two dimensions. On the contrary, this phenomenon is sensitive to slope topography and to effective mechanical properties. The internal friction to be used in the model can be taken directly from the laboratory measurements. The effective cohesion value c is not well constrained by the measurements; it is constrained by the models themselves that provide the c value at which the instability is initiated. The fact that this value (~1 MPa in the case of the La Clapière area) is within the range of the measured values (0.2 and 2 MPa) further supports the approach used. It follows that it can predict quite reliably the sites where the destabilization may occur and explore its future evolution.

The reported results support the deep normal faulting and associated sagging/sacking previously obtained on the physical models (Chemenda et al., 2005; Bachmann et al., 2006) in which virtually the same principle (a progressive homogeneous reduction of the cohesion) was applied to destabilize the "mountain". The model geometry, properties of the analogue material, and boundary conditions at the model bottom (which was partially coupled to the rigid base) were, however, not the same as in the presented numerical simulations. Therefore the shallow (La Clapière-type) landslide was not generated in the physical models. It was not generated in the numerical model in Fig. 7 with idealized linear slope topography (the same as in the physical model) either.

The rate of the sagging (of the displacement along the deep normal faults) in the numerical models is much less (more than one to two orders of magnitude) than that of shallow landsliding. The timescale is very different as well: the normal faulting and associated sagging in the presented models start well before and continue after the shallow landsliding. One can suppose that many shallow events can successively occur during the continuing sagging.

References

Ambrosi, C., Crosta, G.B., 2006. Large sackung along major tectonic features in Central Italian Alps. Eng. Geol. 83, 183–200.
Arora, V.K., 1987. Strength and deformational behaviour of jointed rocks. PhD thesis, IIT Delhi, India.
Bachmann, D., Bouissou, S., Chemenda, A., 2006. Influence of large scale topography on gravitational rock mass movements: new insights from physical modeling. Geophys. Res. Lett. 33, L21406. doi:10.1029/2006GL028028.
Bogdanoff, S., 1986. Evolution de la partie occidentale du massif cristallin externe de l'Argentera. Place dans l'arc alpin. Géol. Fr. 4, 433–453.
Casson, B., Delacourt, C., Allemand, P., 2005. Contribution of multi-temporal remote sensing images to characterize landslide slip surface—application to the La Clapière landslide (France). Natural Hazards and Earth System Sciences, vol. 5, pp. 425–437.
Chemenda, A.I., 2007. The formation of shear-band/fracture networks from a constitutive instability: theory and numerical experiment. J. Geophys. Res. 112, B11404. doi:10.1029/2007JB005026.
Chemenda, A., Bouissou, S., Bachmann, D., 2005. 3-D Physical modeling of deep-seated landslides: new technique and first results. J. Geophys. Res. 110, F04004. doi:10.1029/2004JF000264 No. F4.
Chen, W.F., Han, D.J., 1988. Plasticity for Structural Engineers. Springer-Verlag, New York.
Chigira, M., 2001. Micro-sheeting of granite and its relationship with landsliding especially after the heavy rainstorm in June 1999, Hiroshima prefecture. Jpn. Eng. Geol. 29, 219–231.

Delteil, J., Stephan, J.F., Attal, M., 2003. Control of Permian and Triassic faults on Alpine basement deformation in the Argentera massif (external southern French Alps). Bull. Soc. Geol. Fr. 174, 55–70.

Follacci, J.P., 1987. Les mouvements du versant de La Clapière à Saint Étienne de Tinée (Alpes Maritimes). Bull. Lab. Ponts Chaussées 220, 107–109.

Follacci, J.P., 1999. Seize ans de surveillance du glissement de La Clapière (Alpes Maritimes). Bull. Lab. Ponts Chaussées 220, 35–51.

Guglielmi, Y., Vengeon, J.-M., Bertrand, C., Mudry, J., Follacci, J.-P., Giraud, A., 2002. Hydrogeochemistry: an investigation tool to evaluate infiltration into large moving rock masses (case study of La Clapière and Séchilienne alpine landslides). Bull. Eng. Geol. Environ. 61, 311–324.

Guglielmi, Y., Cappa, F., Binet, S., 2005. Coupling between hydrogeology and deformation of mountainous rock slopes: insights from La Clapière area (southern Alps, France). C. R. Geosciences 337, 1154–1163.

Gunzburger, Y., Laumonier, B., 2002. Origine tectonique du pli supportant le glissement de terrain de la Clapière (NordOuest du massif de l'Argentera–Mercantour, Alpes du Sud, France) d'après l'analyse de la fracturation. C. R. Geosciences 334, 415–422.

Gunzburger, Y., Merrien-Soukatchoff, V., 2002. Caractérisation mécanique d'un versant rocheux instable au moyen du système RMR-Cas de la Clapière (Alpes-Maritimes). Symposium International Param2002, Identification et détermination des para-mètres des sols et des roches pour les calculs géotechniques, September 2–3, Paris, France, pp. 541–548.

Gunzburger, Y., Merrien-Soukatchoff, V., Guglielmi, Y., 2005. Influence of daily surface temperature fluctuations on rock slope stability: case study of the Rochers de Valabres slope (France). Int. J. Rock Mech. Min. Sci. 42, 331–349.

Hajiabdolmajid, V., Kaiser, P.K., Martin, C.D., 2002. Modelling brittle failure of rock. Int. J. Rock Mech. Min. Sci. 39, 731–741.

Hall, K., André, M.F., 2001. New insights into rock weathering from high-frequency rock temperature data: an Antarctic study of weathering by thermal stress. Geomor-phology 41, 23–35.

Helmstetter, A., Sornette, D., Grasso, J.-R., Andersen, J.V., Gluzman, S., Pisarenko, V., 2004. Slider-block friction model for landslides: application to Vaiont and LaClapìere landslides. J. Geophys. Res. 109, B02409. doi:10.1029/2002JB002160.

Hermanns, R.L., Blikra, L.H., Naumann, M., Nilsen, B., Panthi, K.K., Stromeyer, D., Longva, O., 2006. Examples of multiple rock-slope collapses from Köfels (Ötz valley, Austria) and western Norway. Eng. Geol. 83, 94–108.

Hill, S.E., Rosenbaum, M.S., 1998. Assessing the significant factors in a rock weathering system. Quart. J. Eng. Geol. Hydro. 31, 85–94.

Hoek, E., Bray, J.W., 1991. Rock Slope Engineering. Elsevier Science Publishing, New York. 358 pp.

Hoek, E., Brown, E.T., 1997. Practical estimates of rock mass strength. Int. J. Rock Mech. Min. Sci. 8, 1165–1186.

Ivaldi, J.-P., Guardia, P., Follacci, J.-P., Terramorsi, S., 1991. Plis de couverture en echelon et failles de second ordres associés à un décrochement dextre de socle sur le bord nord-ouest de l'Argenterra (Alpes-Maritimes, France). C.R. Acad. Sci. Paris serie II 313, 316–368.

Jomard, H., 2006. Analyse multi-échelles des déformations gravitaires du Massif de l'Argentera Mercantour. Ph.D Thesis, Departement des sciences de la terre et de l'univers, Univ. Nice Sophia Antipolis, Nice, France, 246 pp.

Lebourg, T., Binet, S., Tric, E., Jomard, H., El Bedoui, S., 2005. Geophysical survey to estimate the 3D sliding surface and the 4D evolution of the water pressure on part of a deep seated landslide. Terra Nova 17, 399–406.

Maréchal, J.C., Wyns, R., Lachassagne, P., Subrahmanyan, K., Touchard, F., 2003. Anisotropie verticale de la perméabilité de l'horizon fissuré des aquifères de socle: concordance avec la structure géologique des profils d'altération. C. R. Geosciences 335, 451–460.

Marti, J., Cundall, P.A., 1982. Mixed discretization procedure for accurate solution of plasticity problems. Int. J. Num. Methods Anal. Methods Geomech. 6, 129–139.

Merrien-Soukatchoff, V., Gunzburger, Y., 2006. Models available to understand failure and pre-failure behaviour of large rock slope movement: the case of La Clapière, Southern Alps, France. In: Evans, Stephen G., Mugnozza, Gabriele Scarascia, Strom, Alexander, Hermanns, Reginald L. (Eds.), Landslides from Massive Rock Slope Failure. Springer, Berlin. ISBN: 1-4020-4036-9.

Merrien-Soukatchoff, V., Quenot, X., Guglielmi, Y., 2001. Modélisation par éléments distincts du phénomène de fauchage gravitaire. Application au glissement de La Clapière (Saint-Etienne-de-Tinée, Alpes Maritimes). Rev. Fr. Géotech. 95/96, 133–142.

Migon, P., Lidmar-Bergstroem, K., 2002. Deep weathering through time in central and northwestern Europe: problems of dating and interpretation of geological records. Catena 49, 25–40.

Pellegrino, A., Prestininzi, A., 2007. Impact of weathering on the geomechanical properties of rocks along thermal-metamorphic contact belts and morpho-evolutionary. Geomorphology 87, 176–195.

Verman, M., Singh, B., Viladkar, M.N., Jethwa, J.L., 1997. Effect of tunnel depth modulus of deformation of rock mass. Rock Mech. Rock Eng. 30, 121–127.

Willenberg, H., 2004. Geologic and kinematics model of a complex landslide in crystalline rock (Randa, Switzerland), Ph.D Thesis, Swiss Federal Institute of Technology, Zurich.

Wong, T.-F., David, C., Zhu, W., 1997. The transition from brittle faulting to cataclastic flow in porous sandstones: mechanical deformation. J. Geophys. Res. 102, 3009–3025.

Wyns, R., 2002. Climat, eustatisme, tectonique: quels contrôles pour l'altération continentale ? Exemple des séquences d'altération cénozoïques en France. Bull. Inf. Géol. Bassin Paris 39, 5–16.